Applied Catalysis B: Environmental 342 (2024) 123430

Contents lists available at ScienceDirect

Applied Catalysis B: Environmental

journal homepage: www.elsevier.com/locate/apcatb

Design of bimetallic catalyst with dual-functional Cu-Ce sites for synergistic NO_X and toluene abatement

Ziyang Guo [a], Beilong Lin [a], Yu Huang [a], Jiali Tang [a], Peirong Chen [a,b,c], Daiqi Ye [a,b,c], Yun Hu [a,b,c,*]

[a] School of Environment and Energy, South China University of Technology, Guangzhou 510006, PR China
[b] Guangdong Provincial Key Laboratory of Atmospheric Environment and Pollution Control, Guangzhou 510006, PR China
[c] Guangdong Provincial Engineering and Technology Research Centre for Environmental Risk Prevention and Emergency Disposal, Guangzhou 510006, PR China

ARTICLE INFO

Keywords:
Vanadium-free catalyst
Synergistic elimination
NH_3-SCR
VOCs oxidation

ABSTRACT

Nitrogen oxides (NO_x) and volatile organic compounds (VOCs) coexist in the flue gases from coal-fired power plants and iron/steel smelting industry. In this study, a dual-site catalyst, composed of Cu-Ce-Ti mixed oxide, was screened for the synergistic elimination of NO_x and VOCs. The catalyst showed a synergistic removal efficiency above 95% for both C_7H_8 and NO at 250 °C, and sustain the NO_x and VOCs removal efficiencies above 90% even in the presence of 5 vol% H_2O and 500 ppm SO_2 at 300 °C. Mechanistic studies revealed that the Cu and Ce sites play individual roles in toluene oxidation and NO_x reduction, respectively. The primarily occurred SCR reaction facilitated electron exchange through the redox cycling between Ce^{4+}/Ce^{3+} and Cu^{2+}/Cu^{+} pairs, resulting in a high abundance of Cu^{2+} sites being highly active in toluene oxidation. This study could provide new strategy for high-performance catalysts toward synergistic NO_x and VOCs abatement.

1. Introduction

Nitrogen oxides (NO_x) and volatile organic compounds (VOCs) are crucial precursors of ozone and $PM_{2.5}$ pollution [1–3]. VOCs with concentrations from ppb to ppm often coexist with NO_x in flue gases from coal-fired power plants, cement industry, and steel smelting industry [4,5]. NH_3-assisted selective catalytic reduction (NH_3-SCR) and catalytic oxidation are the mainstream control methods in industry to abate NO_x and VOCs, respectively [3,6]. However, abatement of NO_x and VOCs with separated units has the drawbacks of high equipment investment, large areas occupation and high operating costs. In light of the current focus on multi-pollutant control, the synergistic elimination of NO_x and VOCs in SCR units represents a more energy-efficient and cost-effective alternative [7–10].

Typically, vanadium-based catalysts (V_2O_5-WO_3/TiO_2 and V_2O_5-MoO_3/TiO_2) are used in NH_3-SCR, while noble metal (Pt, Pd) oxides and transition metal (Mn, Fe, Cu, Co) oxides are generally used in VOCs catalytic oxidation [3,6]. For the synergistic elimination of NO_x and VOCs, VTi based catalysts have potential to be used due to their suitable acidity and redox properties [7,9,11,12]. Our research [13] found that VTi based catalysts exhibited 94% toluene conversion at 350 °C, but numerous by-products were formed during reaction, which limited CO_2 selectivity. Doping noble or transition metals can enhance the oxidation ability. For instance, Cu-doped VWTi catalyst displayed an excellent toluene oxidation activity, with 99% conversion and selectivity at 350 °C [14]. Pd-modified VTi catalysts achieved complete conversion of benzene and nitrogen oxides at 350 °C [15]. However, vanadium-based catalysts still have problems of narrow temperature windows, high activation temperatures for the removal of VOCs and high biotoxicity of vanadium [13,16,17]. Therefore, a non-vanadium-based catalyst that is more energy-efficient and environmentally friendly for the synergistic removal of VOCs and NO_x is expected.

On the other hand, catalyst deactivation in multi-pollution control is an issue that should be considered in catalyst design. The deactivation of the catalyst limits its application in practice. The deactivation is mainly due to the competitive adsorption of nitrogenous compounds and organic compounds, active sites inhibition and the side reactions [8,18,19]. In order to solve this problem, catalyst with bimetallic active sites was developed for NOx and VOC abatement, where oxidation and reduction reactions can take place at separate sites to minimize interaction. For metal oxide selection, both effectiveness and greenness were taken into consideration. In the aspect of green chemistry, low

* Corresponding author at: School of Environment and Energy, South China University of Technology, Guangzhou 510006, PR China.
E-mail address: huyun@scut.edu.cn (Y. Hu).

https://doi.org/10.1016/j.apcatb.2023.123430
Received 19 August 2023; Received in revised form 6 October 2023; Accepted 21 October 2023
Available online 24 October 2023

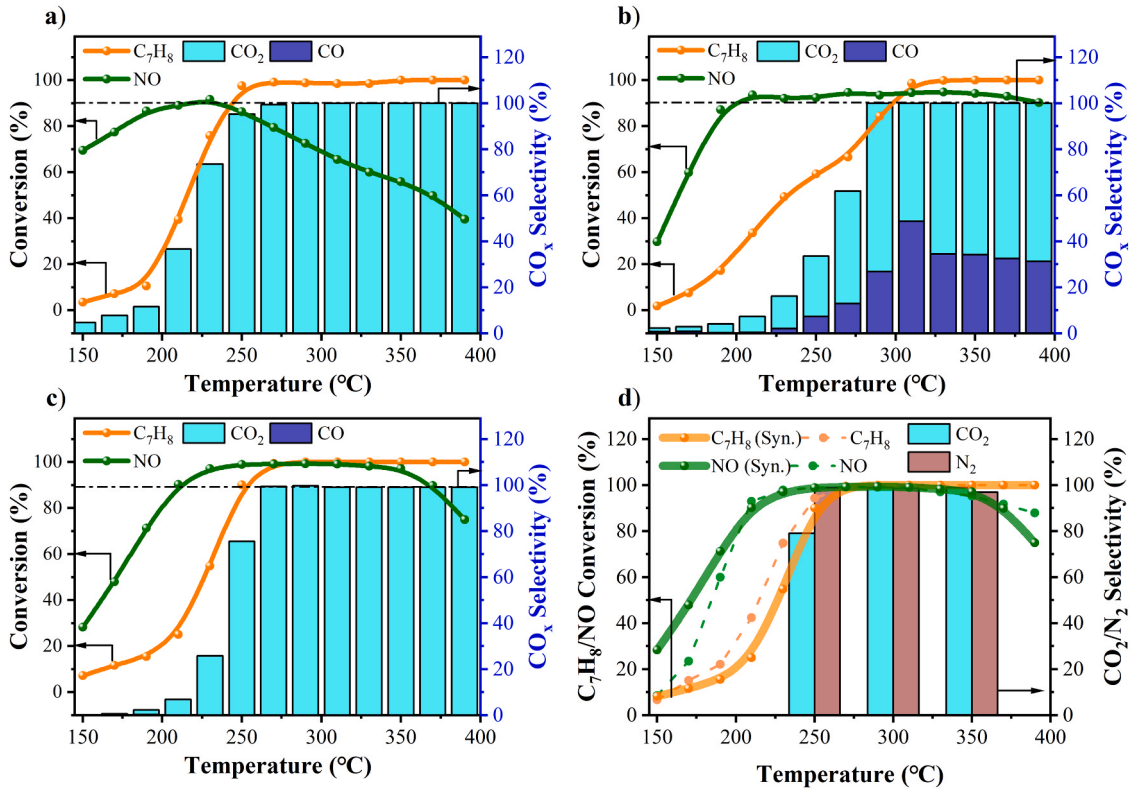

Fig. 1. Toluene conversion, NO_x conversion and CO_x selectivity on (a) CuTi, (b) CeTi, (c) CuCeTi and synergistic C_7H_8 and NO_x abatement performance on CuCeTi catalyst. Reaction conditions: $[C_7H_8] = 50$ ppm, $[NO] = [NH_3] = 500$ ppm, $[O_2] = 10$ vol%.

environmental hazards and abundant metal resources is more preferential to be used, such as abundant Cu and Fe metals [20]. Multi-metal catalysts with tunable redox ability are beneficial to synergistic catalysis, such as Ce, Co and Zr [10]. Earth abundant Cu oxides and non-toxic Ce oxides are worth studying due to their moderated redox ability and tunable physicochemical properties [21–23]. Previous studies focus on their individual performance in VOC oxidation [24,25] and NH_3-SCR process [26,27] respectively, while their synergistic catalytic performance, particularly their role in synergistic reactions was rarely reported.

In this study, Cu oxides and Ce oxides with TiO_2 as support (*i.e.* CuTi, CeTi and CuCeTi) were prepared to investigate the domains effects in synergistic removal performance. The toluene was selected as targeted pollutants for VOCs in the synergistic reaction, as it took up a large proportion and had high potential for total ozone formation [28,29]. Combined with physicochemical characterization and *in situ* diffuse reflection infrared Fourier transform spectroscopy (*in situ* DRIFTS) results, the synergistic reaction mechanism on CuCeTi were illustrated.

2. Experimental section

2.1. Catalyst preparation

Three types of TiO_2-based catalysts with different metal oxides as active sites (*e.g.* Ce site, Cu site and Cu-Ce site) were synthesized by a coprecipitation method. For Cu-Ce site catalyst, the Cu/Ce molar ratio was 0.25. And the mass ratio of Ti/([Cu]+[Ce]+[Ti]) was 50 wt%. For Cu site and Ce site catalysts, the mass ratio of Ti/([Cu or Ce]+[Ti]) site was 50 wt%. The obtained $Cu_{0.5}Ti_{0.5}O_{2-\delta}$, $Ce_{0.5}Ti_{0.5}O_{2-\delta}$ and $Cu_{0.1}Ce_{0.4}Ti_{0.5}O_{2-\delta}$ mixed oxide catalysts were labeled as CuTi, CeTi and CuCeTi, respectively. Full details of the catalyst preparation process are shown in the Supplementary material.

2.2. Material characterizations

X-ray diffraction (XRD), transmission electron microscopy (TEM), inductively coupled plasma atomic emission spectrometry (ICP-OES), Brunauer-Emmett-Teller (BET), X-ray photoelectron spectroscopy (XPS), temperature-programmed desorption (TPD), and temperature-programmed reduction (TPR) were used to characterize the catalysts. *In situ* DRIFTS was used to analyze the catalytic reaction mechanism. Full details are provided in the Supplementary material.

2.3. Catalytic activity evaluation

A home-built fixed bed reactor (Fig. S1) was used to evaluate the catalyst activity. In the detection system, the gas stream out of reactor went into a three-way valve, where gas was divided into GC and flue gas analyzer respectively. Toluene, CO and CO_2 were detected by GC. The NO and NO_2 were detected by flue gas analyzer. Full details of the measurement method, reaction condition and calculation equation are provided in the Supplementary material.

3. Results and discussion

3.1. Catalytic performance

3.1.1. Catalytic activity for NO/C_7H_8 elimination

A series of non-noble metals (Cu, Ce, Co, Fe, Zr) bimetallic catalysts was synthesized and evaluated in the NO/C_7H_8 elimination reaction. Among them, the bimetallic CuCeTi catalyst exhibited the highest NO_x and C_7H_8 conversions (Fig. S2). The mass ratio of Ti in CuCeTi were optimized, and the 50 wt% of TiO_2 (50% CuCeTi) demonstrated the best performance in terms of NO_x/C_7H_8 conversion (Fig. S3) and thus investigated further. The bimetallic CuCeTi catalyst also outperformed the single-component catalysts, namely CuTi and CeTi. In NO/C_7H_8 elimination tests, the CuTi (Fig. 1**a**) achieved 90% toluene conversation

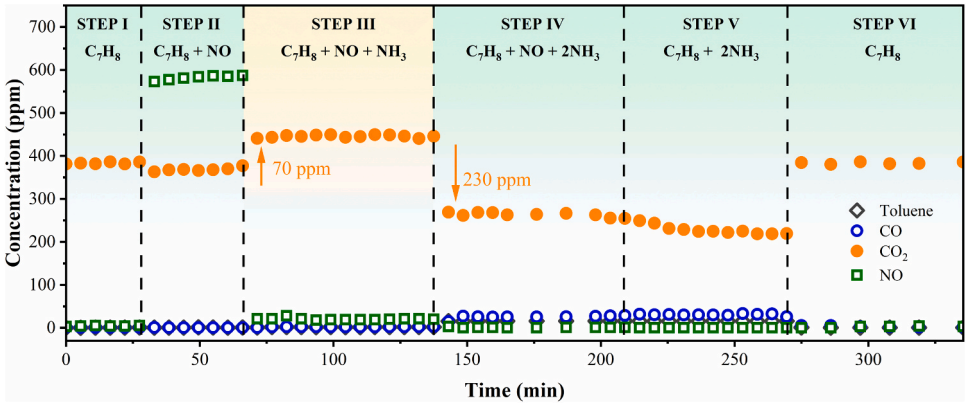

Fig. 2. Transient test of oxidation of toluene on CuCeTi catalyst at 250 °C. Step I: C_7H_8 (50 ppm), Step II: C_7H_8 (50 ppm) and NO (500 ppm), Step III: C_7H_8 (50 ppm), NO (500 ppm) and NH_3 (500 ppm), Step IV: C_7H_8 (50 ppm), NO (500 ppm) and NH_3 (1000 ppm), Step V: C_7H_8 (50 ppm) and NH_3 (1000 ppm), Step VI: C_7H_8 (50 ppm). Reaction conditions: $[C_7H_8]$ = 50 ppm, [NO] = 500 ppm, $[NH_3]$ = 500–1000 ppm when used, $[O_2]$ = 10 vol%.

at a temperature (T_{90}) of approximately 240 ℃, which was higher than that of CeTi (T_{90} = 296 ℃). As a result of the incomplete toluene oxidation, CO was generated on CeTi leading to low CO_2 selectivity (Fig. 1**b**). Cu dopants can enhance the oxidation activity, where CuCeTi (Fig. 1**c**) exhibited a T_{90} of 257 ℃ without CO generation. In terms of NO reduction, CeTi displayed a better performance than CuTi.

Under synergistic reaction conditions (coexistence of toluene, NO and NH_3), a synergistic removal window (namely over 90% toluene and NO_x conversions) of 120 °C (250–370 °C) was observed over the CuCeTi catalyst (Fig. 1**d**). On the contrary, CuTi could not form an effective synergistic NO and C_7H_8 removal window, that of CeTi was found to be above 300 °C (Fig. S4). The 24 h stability tests were performed over CuCeTi at the temperature (250, 300 and 350 ℃) within the synergy window (Fig. S5). The CO_2 selectivity of CuCeTi reached 100% at 300 ℃, and remained constant at higher temperatures, indicating all the organic compounds were converted to CO_2. The N_2O concentration is low, thereby result in over 95% N_2 selectivity across synergy temperature window. Furthermore, the NO_x/C_7H_8 conversion under synergistic conditions was not greatly affected, C_7H_8 T_{90} decreased 9 ℃ and NO T_{90} only decreased 5 ℃. In addition, the CuCe catalyst without Ti oxide displayed toluene T_{90} of 238 ℃ (Fig. S6), which was slightly lower than that of CuCeTi (254 ℃). And the TiO_2 displayed poor NO_x/C_7H_8 conversion (Fig. S7), with less than 50% toluene conversion and near-zero NO conversion at 400 ℃. When the catalysts were tested in a 24 h

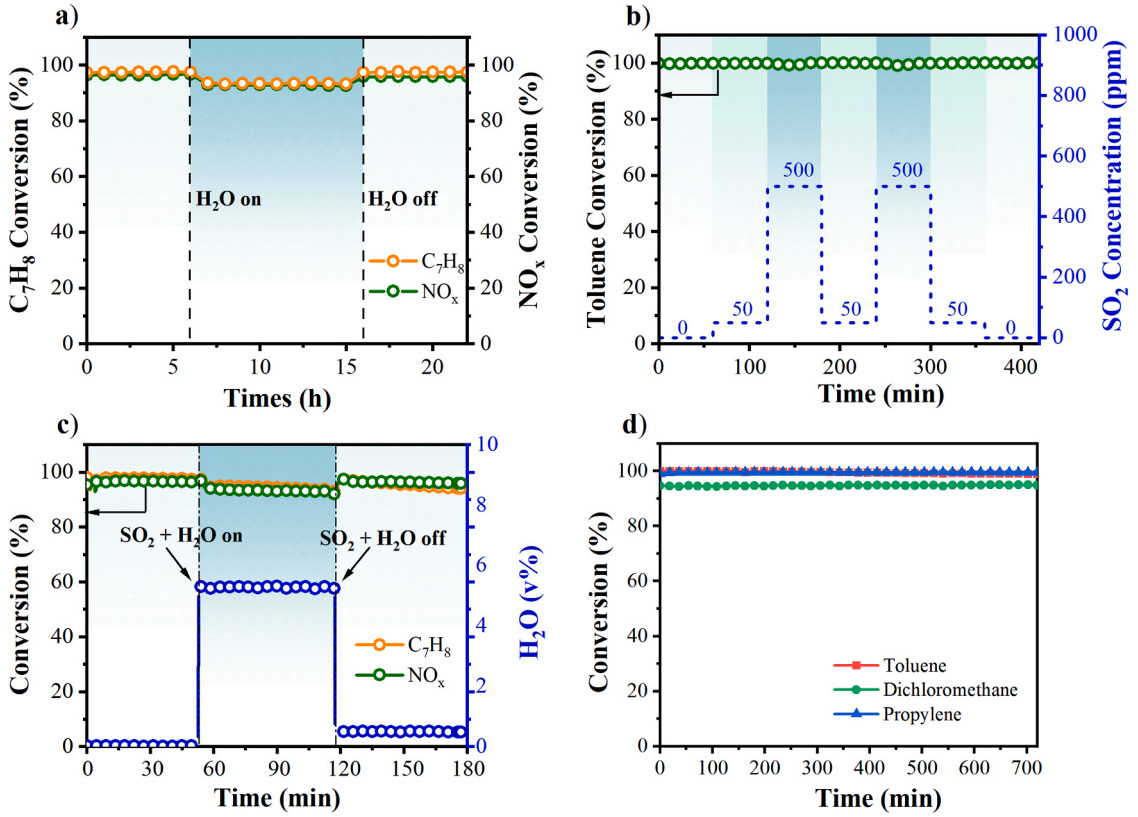

Fig. 3. Catalytic performance of CuCeTi catalyst under (a) 5 vol% H_2O, (b) SO_2 shock resistance test and (c) 5 vol% H_2O and 500 ppm SO_2 simulated flue gas. (d) Conversion of different VOCs on CuCeTi catalyst. Reaction conditions: $[C_7H_8]$ = 50 ppm, [NO] = $[NH_3]$ = 500 ppm, $[SO_2]$ = 0–500 ppm, $[O_2]$ = 10 vol%, H_2O= 5 vol% when used.

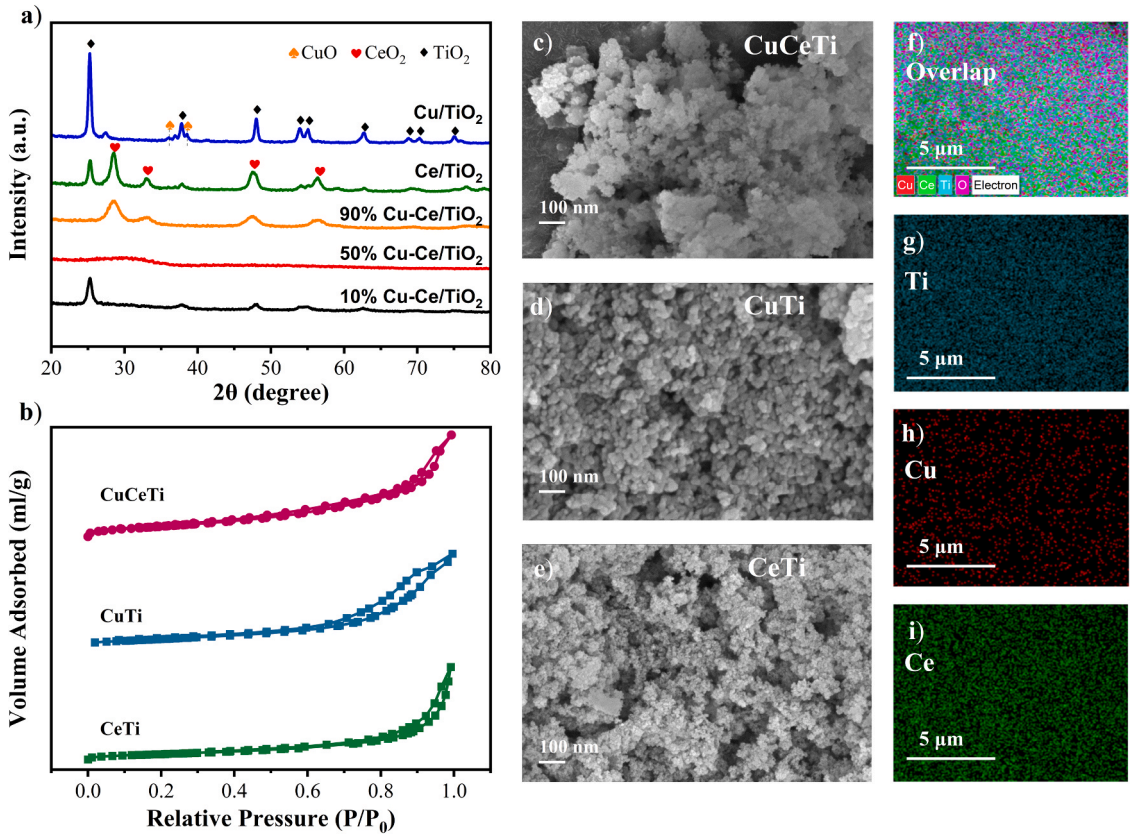

Fig. 4. (a) XRD patterns and (b) N_2 adsorption-desorption isotherms of CuCeTi series catalysts. SEM images of (c) CuCeTi, (d) CuTi and (e) CeTi. (f-i) Elemental mapping of CuCeTi.

experiment under synergistic conditions (Fig. S8), the toluene conversion of the CuCe catalyst started to decrease after 3 h and decreased by about 10% after 24 h of reaction. But the toluene conversion of CuCeTi hardly decreased after 24 h test. Thus, the Ti oxide in the catalytic system was mainly considered to act as a support or cocatalyst to improve the stability of the catalyst [30]. CuCeTi had more potential for use in practical applications with a longer service life. It is noteworthy that the CuCeTi catalyst also had the lowest activation energy (E_a) for toluene oxidation in both single and synergistic conditions (Fig. S9 and Table S1). The turnover frequency (TOF) of the CuCeTi catalyst under synergistic conditions was 11.5×10^4 s^{-1}, which is almost two times higher than that of the CuTi and CeTi catalysts.

3.1.2. *Transient study for gas component influence*

To assess the influence of each gas component (NO, NH_3, and C_7H_8) on the synergistic elimination of toluene and NO by the CuCeTi catalyst, transient tests were conducted by introducing different gas components into the reaction at 250 °C (Fig. 2). At the beginning, 50 ppm of toluene and 10% O_2 atmosphere was passed through catalyst (STEP I). At this point, no toluene was detected and the CO_2 selectivity was 90.4%. Subsequently, 500 ppm of NO was added (STEP II). NO shows nearly no effect on toluene oxidation. When a stoichiometric amount of NH_3 was introduced (STEP III), the NO concentration reduced rapidly as SCR reaction occurred. It was worth to noting that the CO_2 selectivity increased to 99% at this stage. This observation suggested that the presence of SCR reaction in the system enhanced the deep oxidation of toluene. This enhancement could result from a dynamic equilibrium between toluene oxidation and NO reduction, whereby the active sites which participated in the SCR were oxidized, and subsequently derived the toluene oxidation through the reduction of active sites. This observation was in concordance with the finding that the E_a value of CuCeTi catalyst under synergistic conditions (25.8 kJ/mol) is lower than that of under single condition (31.2 kJ/mol). Notably, this promotion phenomenon was not observed on the single-component catalyst CuTi and CeTi (Fig. S10).

Upon introducing two equivalent NH_3 into the reaction (STEP IV), the CO_2 selectivity decreased to 60% with a small amount of CO generated. The decrease in CO_2 selectivity indicated that the presence of excess NH_3 leads to competitive adsorption with toluene, causing occupation of the active site and hindering toluene oxidation. The insufficient oxidation of VOCs would produce CO, the CO cannot undergo further oxidation (combustion) would remain in the flue gas. The inhibition of CO_2 production persisted when only NH_3 was present in the atmosphere (STEP V). Combined with the result from STEP II, implying that NH_3 is the main inhibitor for toluene oxidation. When NH_3 was removed, only toluene remained in the atmosphere (STEP VI). The CO_2 production eventually returned to the initial value, indicating the catalyst has good reproducibility. As the temperature was raised to 300 °C (Fig. S11), the negative effects of NH_3 and NO on the toluene oxidation disappeared. In addition, to investigate the effect of toluene on SCR, different concentrations of toluene were introduced into the NO reduction reaction, and the result showed that there was negligible effect on NO_x conversion (Fig. S12).

3.1.3. *Sulfur/water resistance and stability*

In practical application, H_2O and SO_2 would lead to catalyst poisoning and deactivation. Accordingly, the impact of H_2O and SO_2 on the synergistic removal efficiency of CuCeTi was examined. When 5 vol % of H_2O was introduced to synergistic reaction on CuCeTi at 300 °C, both NO_x and C_7H_8 conversions dropped slightly but still maintained above 95%, and it returned to the initial value after water was removed (Fig. 3**a**). A byproduct N_2O was generated with very low concentration, which was less than 7 ppm (Fig. S13). To assess the SO_2 tolerance of the catalyst, SO_2 shock resistance test was performed by switching SO_2

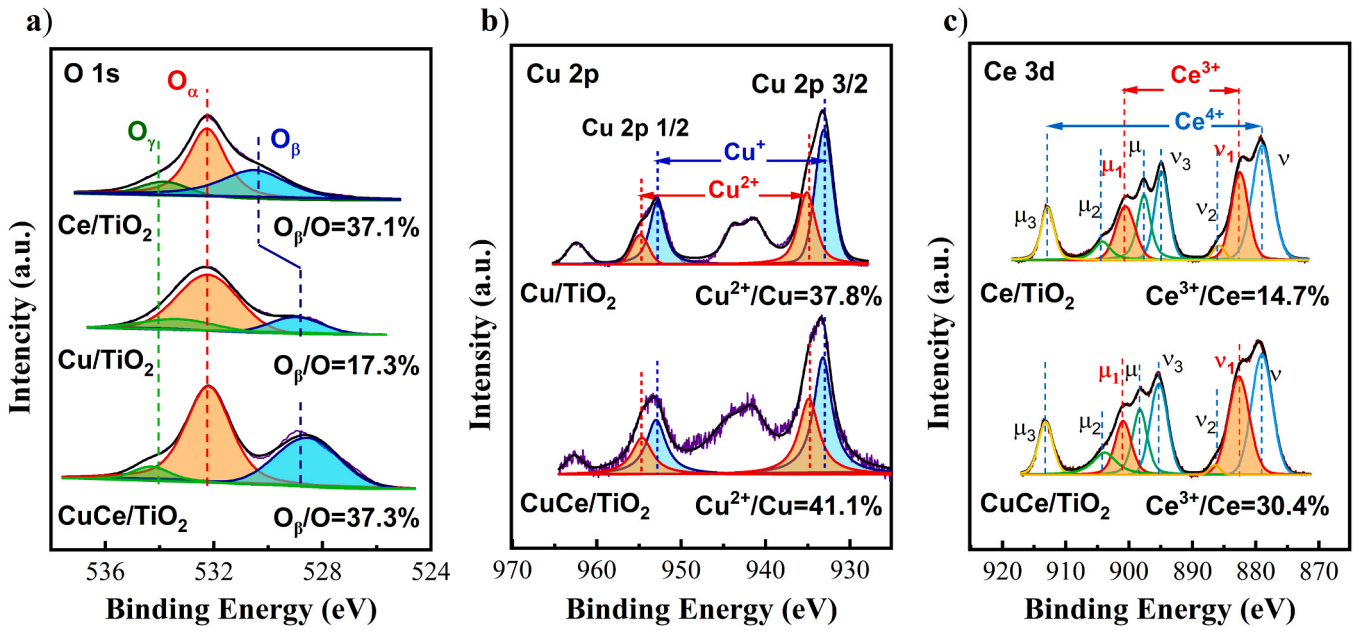

Fig. 5. XPS spectra of (a) O 1 s, (b) Cu 2p, (c) Ce 3d on CuCeTi catalyst.

concentration between 0, 50, and 500 ppm (Fig. 3**b**). The resulting conversion stayed consistently above 95% at 300 °C, indicating the catalyst had good resistance to SO_2 fluctuations. When 5 vol% of H_2O and 500 ppm of SO_2 were simultaneously introduced to CuCeTi at 300 °C (Fig. 3**c**), both toluene and NO_x conversion decreased slightly to around 93%. There was only 2–3% decrease, and the toluene and NO_x conversion returned to 95% when H_2O and SO_2 were removed, indicating that the catalyst was not permanently deactivated. This can be attributed to that the CuCeTi catalyst was able to reduce the adsorption of SO_2 and suppress the oxidation of SO_2. This inhibited the formation of ammonium sulphate, which would lead to physical deactivation of the catalyst [31,32].

The catalytic activity of CuCeTi was also evaluated for other kinds of VOCs (dichloromethane and propene), which are the typical pollutants in fuel gas. The conversion of toluene, dichloromethane and propene under synergistic conditions were all maintained above 95% (Fig. 3**d**), indicating the wide applicability of the CuCeTi catalyst. Furthermore, the FT-IR spectra and XRD of the catalysts before and after the reaction were similar (Fig. S14), which means there was no apparent loss of functional groups or structure change after the H_2O and SO_2 poisoning reaction. Overall, these results show that the CuCeTi catalyst has great potential for industrial applications.

3.2. Physicochemical properties

3.2.1. Characterization of CuCeTi series catalysts

The crystal structure of the CuCeTi series catalysts were identified by XRD (Fig. 4**a**). The position of diffraction peaks at 35.5° and 38.8° were corresponded to CuO (JCPDS, No. 45–0937). The peaks located around 28.6°, 33.1°, 47.5° and 56.4° can be indexed to CeO_2 cubic fluorite structure (JCPDS 43–1002). The typical anatase phase of TiO_2 displaying main diffraction peaks at 25.2°, 37.0°, 37.9°, 48.3°, 54.0°, 54.9°, 62.7°, 68.8°, 70.1° and 75.0° (PDF #21–1272). At lower metal loadings (10% CuCeTi), no CuO and CeO_2 diffraction peaks were observed, which would be due to the small amount of loading evenly dispersed on the surface. 50% CuCeTi has no characteristic peaks, indicating the formation of amorphous oxides. This phenomenon could be result from the enhanced interaction between TiO_2 and Cu-Ce. From the Ti 2p XPS spectra of CuCeTi (Fig. S15), the peaks for Ti^{4+}, Ti^{3+} and Ti^0 were obtained. The Ti^{2+} and Ti^0 species are signatures of oxygen vacancy defects in the structure. This oxygen vacancy would result from a strong interaction between Cu, Ce and Ti, which inhibited crystallization of the CuCeTi [33]. Amorphous oxides have a large number of randomly oriented bonds and surface defects, which can optimize the adsorption/-desorption of reactants to obtain excellent catalytic activity [34]. At higher loading (90%), CuO and CeO_2 diffraction peaks were detected, indicating the formation of corresponding crystal structures on the catalyst surface. However, the intensity of CuO peaks were relatively low, suggesting that copper was highly dispersed on the support surface. Combined with the elemental component analysis results from ICP-OES (Table S2), demonstrating the successful preparation of the CuCeTi series catalyst. From BET result, the CuCeTi series catalysts are characterized as mesoporous catalysts (Table S3). The introduction of Ce results in an increased specific surface area, which makes more active sites exposed to contaminants molecules, thereby enhancing the catalytic activity. The nitrogen isothermal adsorption and desorption curves plotted for CuTi, CeTi, and CuCeTi display typical IV isotherms with H3-type hysteresis loops (Fig. 4**b**). The morphologies of the catalysts are shown in Fig. 4 **(c-e)**, CuTi, CeTi and CuCeTi have granular structures with smooth surfaces and regular morphology, which is conducive to the adsorption, activation and desorption of pollutant molecules in the process of catalytic oxidation. And the elemental mapping (Fig. 4 **f-i** and Fig. S16) reveals that the active components, Cu and Ce, are uniformly dispersed on the catalyst.

3.2.2. Surface chemical properties

The chemical states of the surface elements were analyzed by XPS (Fig. 5) and the compositional ratios are illustrated in Table S4. The O 1 s peaks (Fig. 5**a**) at 530.3, 532.3, and 534.0 eV are attributed to lattice oxygen (O^{2-}, labeled as O_β), chemisorbed oxygen (O_2^-, O_2^{2-}, O^-, labeled as O_α), and adsorbed hydroxyl or H_2O species (labeled as O_γ), respectively [35]. The O_α ratio of CuTi was higher than that of CeTi (Table S4), which is conducive to the adsorption and dissociation of toluene [36]. The higher O_α ratio of CuTi could be due to the enhanced interaction between Cu and Ti species. This interaction could increase amounts of active oxygen species through the promotion of the oxygen vacancies formation [37]. The introduction of Ce site into CuTi resulted in an increase in the O_β ratio from 18% to 37%, indicating that Ce dopants can promote the lattice oxygen formation in the CuCeTi catalyst (consistent with O_2-TPD result in Fig. S17 and Table S5). Lattice oxygen can

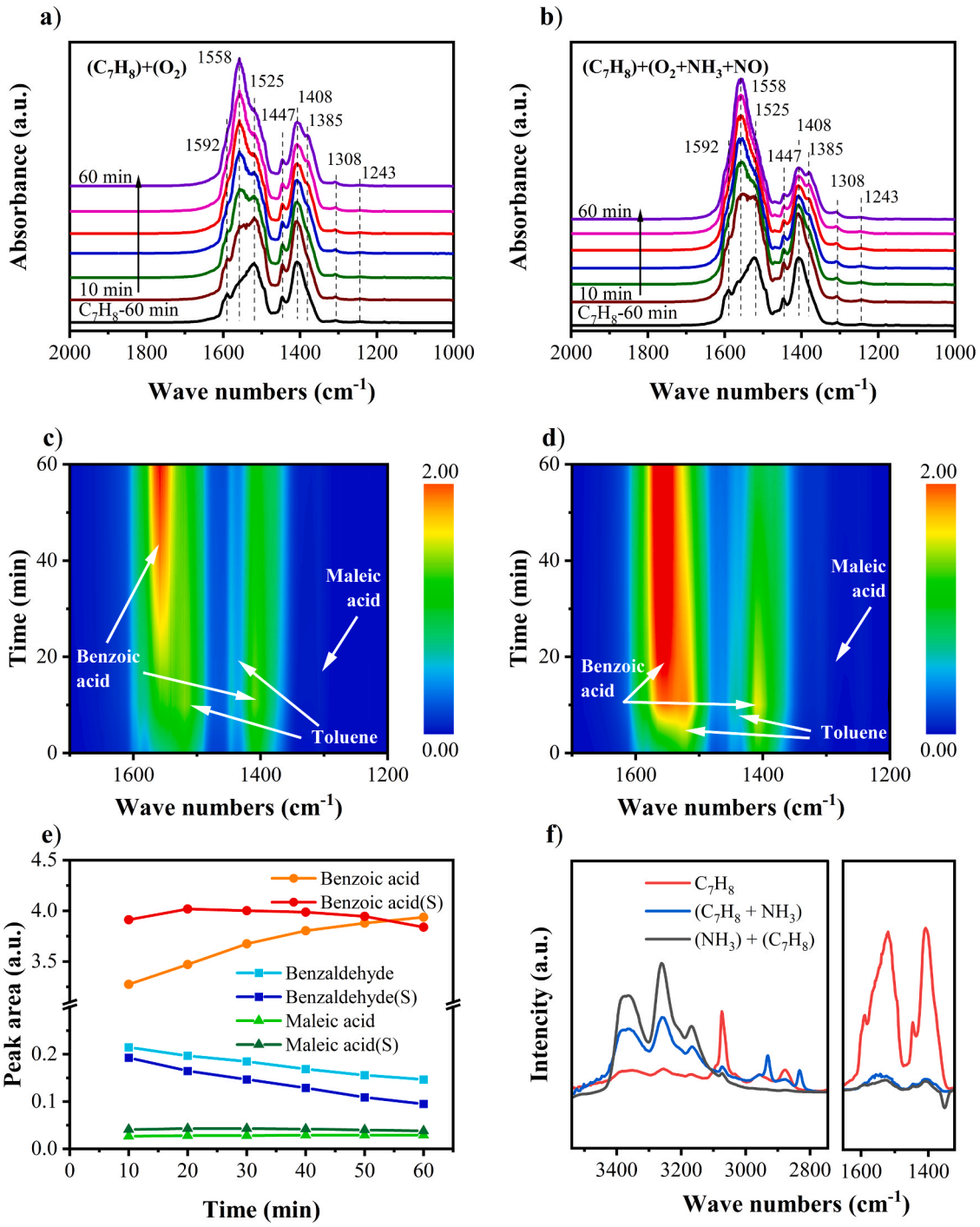

Fig. 6. *In situ* DRIFTS spectra of CuCeTi catalysts at 250 °C with (a, c) (C_7H_8) + (O_2), (b, d) (C_7H_8) + (O_2 + NH_3 + NO), (e) peak areas of intermediate products under single condition and synergistic conditions, (f) C_7H_8 adsorption for 60 min under different conditions.

participate in the toluene oxidation reaction through the Mvk mechanism and contribute to ring-oping reaction [38].

In the Cu 2p spectra (Fig. 5**b**), peaks at 954.2 and 934.4 eV correspond to Cu^{2+} and peaks at 953.0 and 933.2 eV correspond to Cu^{+} [39]. The catalyst surface contained both Cu^{+} and Cu^{2+} with Cu^{+} predominant (Table S4). The introduction of Ce sites resulted in an increase in the Cu^{2+} ratio in the catalyst. This can be attributed to Ce occupying the position of Cu^{+} and altering the physical properties of the catalyst. More Cu^{2+} can be generated through $Ce^{4+} + Cu^{+} \leftrightarrow Ce^{3+} + Cu^{2+}$ reaction [40]. The Cu 2p3/2 binding energies in CuTi had slightly higher Cu 2p3/2 binding energies compared to the Cu_2O and CuO reported in the literature, which could arise from the strong interaction between Cu oxide and Ti oxide support [41]. In addition, Cu^0 was not found according to Cu LMM auger spectroscopy (Fig. S18). This means that Cu^{+} and Cu^{2+} were predominant in the CuCeTi catalyst, so the electron transfer mainly took place with Cu^{+} and Cu^{2+}. In Ce 3d XPS spectra (Fig. 5**c**), the bands labeled u, u2, u3, v, v2 and v3 are attributed to the Ce^{4+} oxidation state, while the peaks labeled u1 and v1 are attributed to Ce^{3+} [42]. The valence state is mainly Ce^{4+} with Ce^{3+} coexisting (Table S4). The introduction of Cu sites resulted in increase of Ce^{3+} ratio from 14.7% to 30.4%. The doubled Ce^{3+} ratio could associated with the generation of oxygen vacancies according to charge compensation [43].

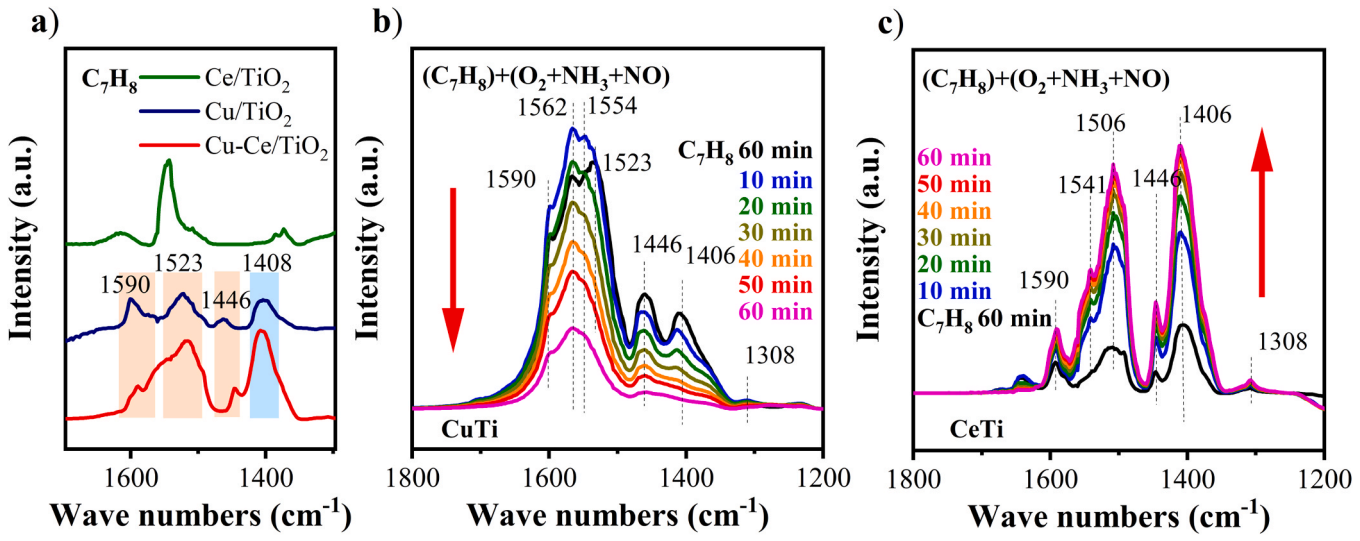

Fig. 7. *In situ* DRIFTS spectra of (a) 60 min C_7H_8 adsorption over different catalyst at 25 °C, (b) CuTi catalysts at 250 °C (c) CeTi catalysts at 250 °C with (C_7H_8) + (O_2 + NH_3 + NO).

The coexistence of Cu and Ce can form Cu-O-Ce solid solutions (also confirmed by XRD and H_2-TPR results in Fig. S19 and Table S6), which produce structural defects and oxygen vacancies [44]. The increase of Cu^{2+} and Ce^{3+} ratio in CuCeTi catalyst indicates that more Cu^{2+}-O-Ce^{3+} species have positive effect in synergistic reaction Moreover, the generation of Cu-O-Ce solid solutions and interaction between Ce^{4+}/Ce^{3+} and Cu^{2+}/Cu^{+} lead to high redox properties [45], which is also beneficial for synergistic reaction.

3.3. Reaction mechanisms

3.3.1. Toluene oxidation reaction process

The *in situ* DRIFTS of the toluene oxidation reaction was performed, toluene was pre-adsorbed on the CuCeTi catalyst followed by introducing O_2 to oxidize toluene from 100° to 400°C (Fig. S20a). The resulting characteristic peaks assigned to different functional groups were listed in Table S8. Toluene was oxidized on the catalyst surface through the pathways of benzyl alcohol, benzaldehyde, benzoic acid, maleic anhydride, small molecule acids, CO_2 and H_2O, which is consistent with other studies [14,45]. During the oxidation reaction, benzoic acid (1407, 1554 cm^{-1}) was the main intermediate product, which accumulated the most as the reaction progressed (Fig. S20b). The decline of benzoic acid was observed at 250 °C, and all other intermediates were rapidly consumed at 300 °C, suggesting that the ring opening of benzoic acid was the rate-determining step of the reaction.

By studying a series of time-resolved *in situ* DRIFTS spectra, the spectra of toluene oxidation under single condition (Fig. 6**a** and **c**) and synergistic conditions (Fig. 6**b** and **d**) were compared. The peak due to toluene (1523 cm^{-1}) was rapidly depleted within 40 min under synergistic conditions (Fig. S21). However, toluene can be still observed under single condition at 60 min, which indicating introduction of NH_3 +NO can facilitate toluene conversion. The peak areas of the major intermediates (benzaldehyde, benzoic acid and maleic acid) under single condition and synergistic conditions were compared in Fig. 6**e**. Benzaldehyde was continuously consumed in the C_7H_8 + O_2 reaction, and the peak area showed a decreasing trend within 60 min. While benzoic acid (1408 and 1558 cm^{-1}) kept accumulating and the peak area showed an increasing trend. Under synergistic conditions, benzoic acid was also generated on the catalyst surface and the peak area meet the maximum point at 20 min. Then the peak area of benzoic acid decreased until it was lower than that of under the single condition at 60 min, indicating that benzoic acid can be generated faster and consumed through the ring-opening reaction more quickly under the synergistic conditions. Furthermore, the lower benzaldehyde and higher maleic acid peak area under synergistic conditions also demonstrated that toluene can be oxidized more rapidly. This could explain the promotion effect on deep toluene oxidation found in the transient test, where the synergistic promotion was achieved by accelerating the conversion of adsorbed toluene to produce more benzoic acid for the ring opening reaction. Followed by more rapid conversion toward small molecule acids after the rate determining step, and finally resulted in more CO_2 and H_2O.

When 500 ppm NH_3 and 50 ppm C_7H_8 were pre-adsorbed on CuCeTi simultaneously (blue line (C_7H_8 + NH_3) in Fig. 6**f**), competitive adsorption of NH_3 and toluene resulted in a weaker signal of toluene adsorption than those observed under single condition. When 50 ppm C_7H_8 were passed on the NH_3 pre-adsorbed CuCeTi (black line (NH_3) + (C_7H_8) in Fig. 6**f**), toluene was difficult to be adsorbed due to NH_3 first coming to the adsorption sites, result in the lowest C_7H_8 adsorption. In Fig. S22, an excess amount of NH_3 (500 ppm NO and 1000 ppm NH_3) were passed on the toluene pre-adsorbed CuCeTi. After 30 min of the excess NH_3 passage, the vibrational peak corresponding to toluene at 3075 cm^{-1} was essentially unchanged, while the characteristic peaks of benzoic acid (1554, 1406 cm^{-1}) decreased. This was in contrast to the synergistic conditions where the toluene decreased and the intermediate product increased. These observations suggested that the excess NH_3 not only affected the adsorption of C_7H_8 but also inhibited the formation of intermediates. This finding matched the results of transient experiments.

To investigate the role of Cu and Ce sites in toluene oxidation, the toluene oxidation was examined over CuTi, CeTi, and CuCeTi catalysts. Since the adsorption of toluene on the catalyst surface is the prerequisite of the oxidation process, the DRIFTS spectra of toluene adsorption on the three catalysts were compared (Fig. 7**a**). The toluene adsorption peak on CuTi was similar to that on CuCeTi, suggesting that the Cu site is the main adsorption site for toluene. During the toluene oxidation reaction, the benzene ring C=C (1600 cm^{-1}) and benzoic acid (1406 cm^{-1}) were observed on CuTi (Fig. S23) and disappeared after 60 min. However, the characteristic peak on CeTi did not change much with the reaction time (Fig. S24), meaning that the conversion of toluene was not complete, which was consistent with the activity test results. The trend of intermediate formation and consumption on CuTi was similar to that on CuCeTi, and maleic acid (1306 cm^{-1}) as the evidence for ring-opening reactions was also observed, suggesting that the Cu site was able to drive the ring-opening reaction toward total oxidation. Under synergistic conditions, CuTi exhibited superior catalytic oxidation performance towards toluene, with the rapid conversion of benzoic acid and

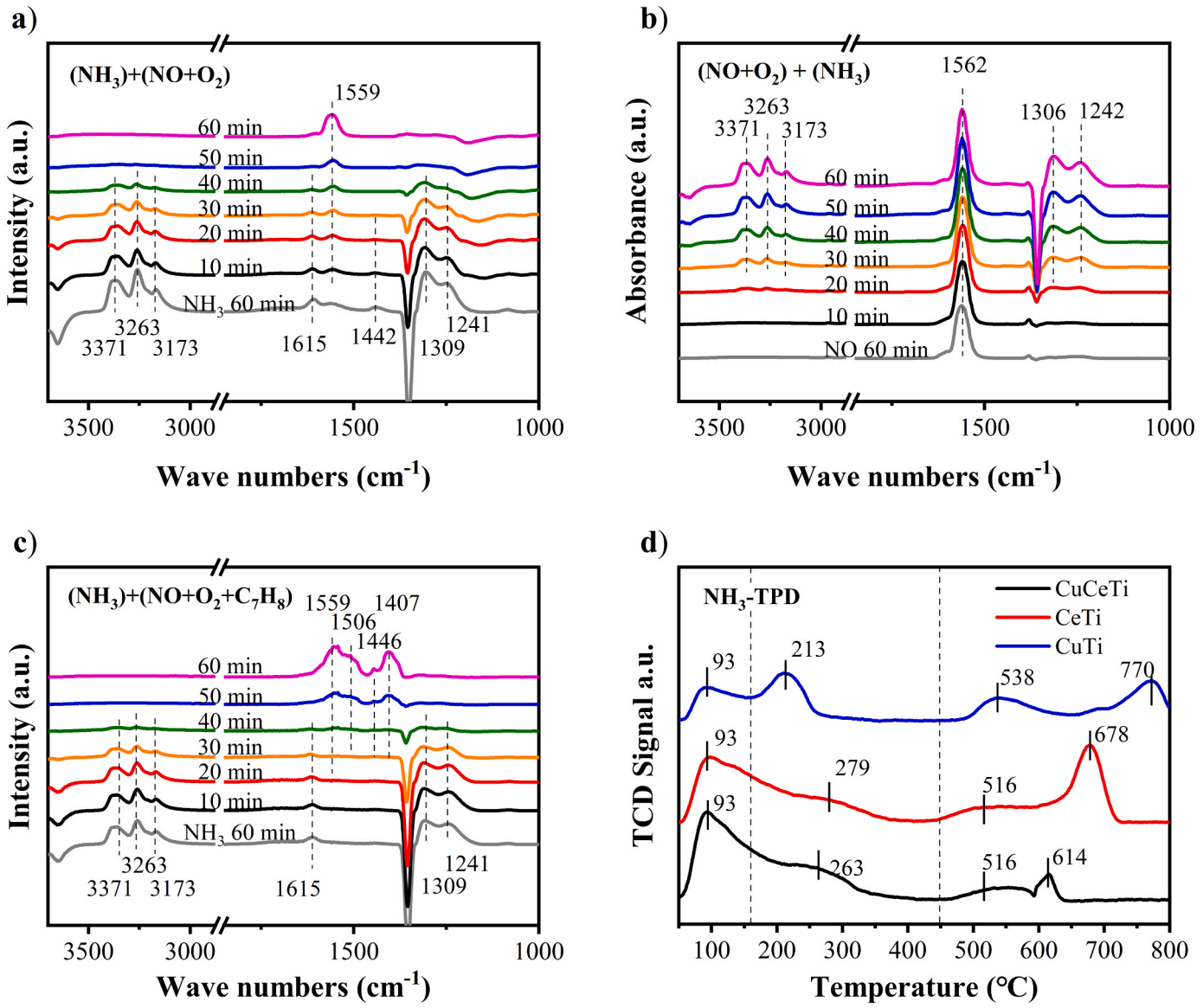

Fig. 8. *In situ* DRIFTS spectra at 250 °C on the CuCeTi catalyst with (a) (NH_3) + ($NO + O_2$), (b) ($NO + O_2$) + (NH_3), (c) (NH_3) + ($C_7H_8 + NO + O_2$) and (d) NH_3-TPD for different catalyst.

maleic acid to H_2O and CO_2 (Fig. 7**b**). On the contract, CeTi demonstrated poor catalytic oxidation activity, with benzoic acid accumulating over time without any discernible decrease (Fig. 7**c**). The conversion tendency of benzoic acid on CuCeTi was consistent with that on CuTi. Therefore, the Cu site is suggested to play a major role in toluene oxidation.

3.3.2. NO_x reduction reaction process

For the catalytic performance in SCR, the pre-adsorption of NH_3 and NO on CuCeTi followed by SCR reaction was studied first. After the adsorption of NH_3 at 250 ℃ (Fig. 8**a**), the adsorption peaks of 1615, 1309 and 1241 cm^{-1} were related to the coordinated NH_3 on Lewis acid site, and the peaks at 1442 cm^{-1} can be assigned to the NH_4^+ species on Brønsted acid site. The bands above 3000 cm^{-1} were attributed to the vibration of N-H on NH_3. The peaks corresponding to NH_3 gradually diminished during the first 40 min, suggesting that the adsorbed NH_3 was consumed by the reaction with NO. After this, NH_3 was depleted at 50 min, and a peak at 1560 cm^{-1} (monodentate nitrate) began to accumulate, indicating that all adsorbed NH_3 was depleted and excess NO remained on the catalyst surface. When $NO+O_2$ was pre-adsorbed for 60 min at 250 °C and then NH_3 was added for 60 min (Fig. 8**b**). The NO peaks remained unchanged, implying that the adsorbed NO was not involved in the SCR reaction. Consequently, in the NH_3-SCR reaction on CuCeTi, the adsorbed NH_3 reacted with gaseous NO instead of adsorbed NO, which following the Eley-Rideal (E-R) mechanism [46, 47].

For the SCR reaction on CuTi (Fig. S25), the peak above 3000 cm^{-1} (vibration of N-H on NH_3) disappeared completely when the reaction proceeded to 30 min. The peaks at 1264 and 1615 cm^{-1} (NH_3 adsorbed on the Lewis acid) also vanished. Instead, the bridging nitrate (1601 cm^{-1}) and bidentate nitrates (1541 cm^{-1}) appeared. In contrast, when SCR was conducted on CeTi (Fig. S26), the peak corresponding to NH_3 almost completely vanished after 20 min, suggesting that faster conversion at 250 °C. Therefore, the Ce site exhibited higher activity than Cu site in SCR reaction.

Under synergistic conditions (Fig. 8**c**), the peaks of NH_3 almost disappeared at 40 min, which was similar to that of the single condition. This was consistent with the conclusion that toluene had almost no effect on SCR found in the activity test (Fig. S12). NH_3-TPD was conducted to explore the amount and acidity of surface acids (Fig. 8**d** and Table S7).

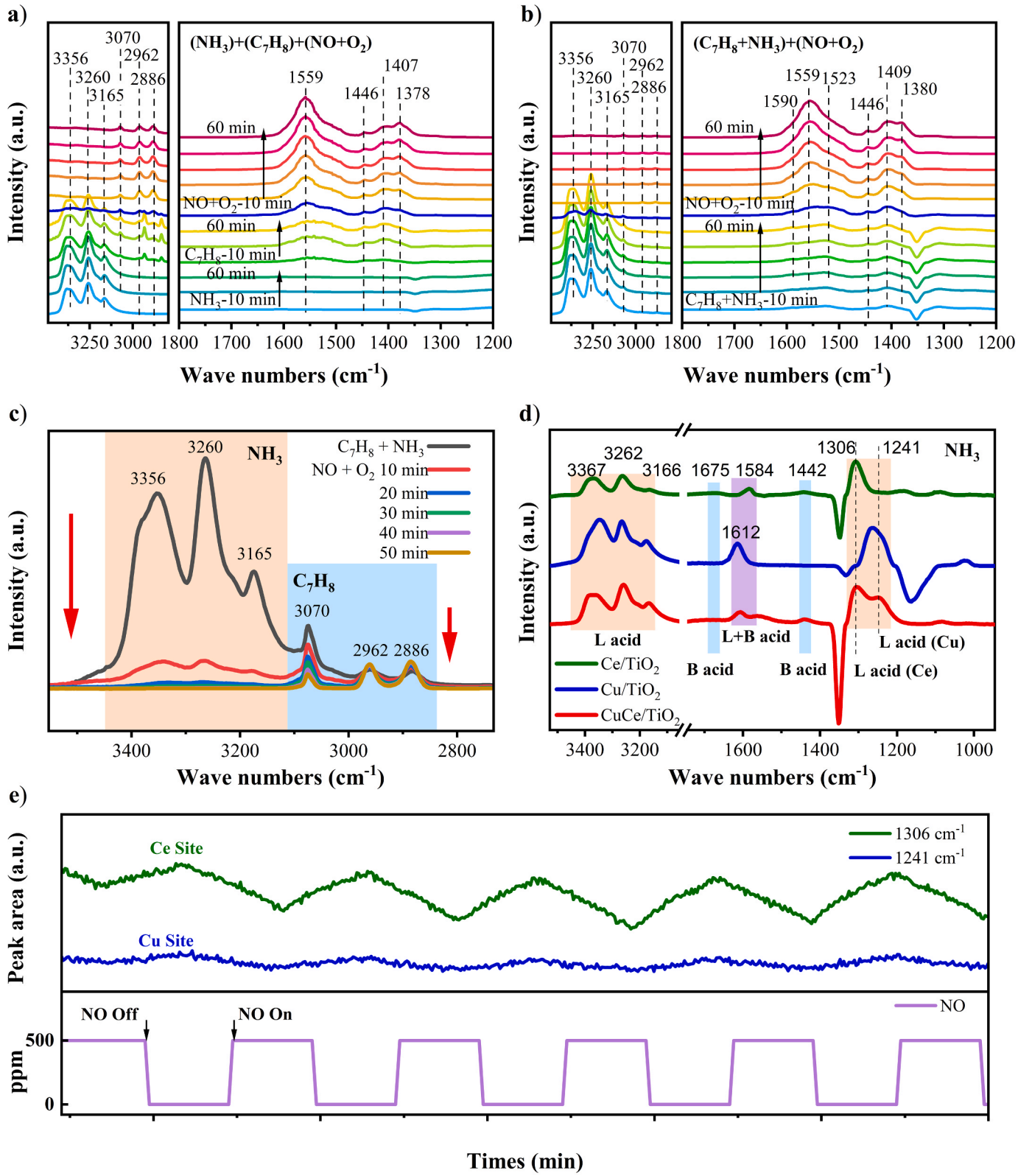

Fig. 9. *In situ* DRIFTS spectra taken at 250 °C on the CuCeTi catalysts upon (a, c) (NH_3) + (C_7H_8) + (NO + O_2), (b) (NH_3 + C_7H_8) + (NO + O_2), (d) NH_3 adsorption on different catalyst at 250 ℃ and (e) the change of NH_3 peak area over CuCeTi during NO switching.

There were two NH_3 adsorption peaks in the range of 70–150 °C and 150–450 °C for both samples, which were assigned to weakly adsorbed ammonia and moderately adsorbed ammonia sites, respectively. These peaks were corresponded to NH_3 adsorption at the Lewis acid sites. Peaks above 450 °C were corresponded to NH_3 adsorption at strong Brønsted acid site [48]. By comparing the NH_3 desorption over three catalysts, the introduction of Cu had a positive effect on creating Lewis acid sites. This was consisting with the finding on NH_3 adsorption

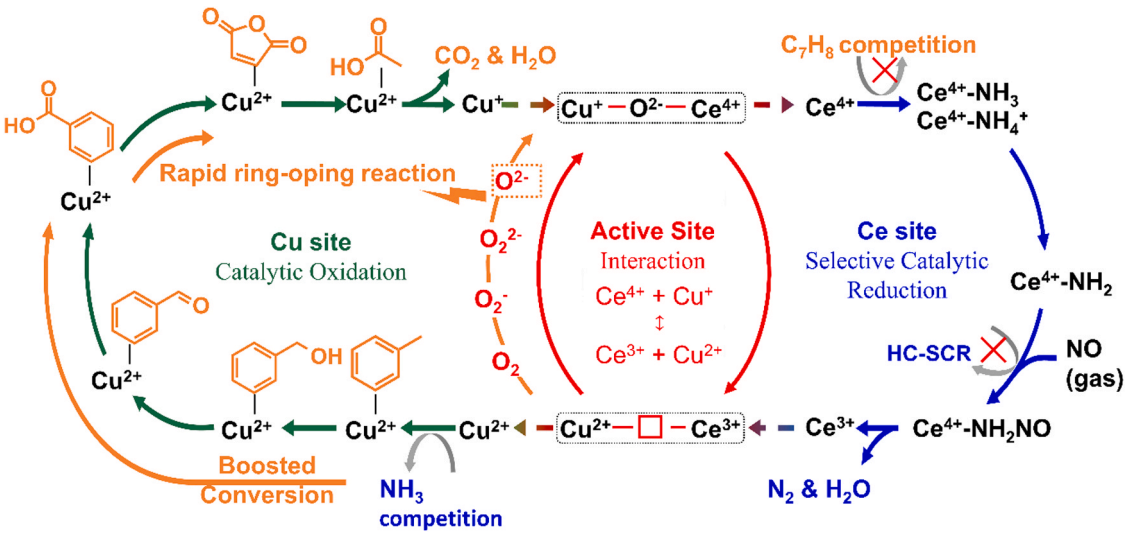

Scheme 1. Proposed synergistic reaction mechanism on CuCeTi.

DRIFTS spectrum at room temperature (Fig. S27). The CuCeTi catalyst that possessed more Lewis acid sites facilitated the adsorption of toluene and NO and the generation of active species [49]. Furthermore, the strong acid peak (614 °C) on CuCeTi shifted to lower temperatures, meaning the NH_3 on Brønsted acid site was more easily activated and facilitated the SCR reaction through the E-R mechanism [50].

Fig. 9 **(a)** and **(b)** shows the *in situ* DRIFTS spectra resulting from the pre-adsorbed of NH_3 followed by C_7H_8, and simultaneous pre-adsorbed of $NH_3 + C_7H_8$. In both spectra, there was no observation of new characteristic peaks and NH_3 eventually disappeared, indicating that the toluene adding sequence did not change the reaction pathway. After NO + O_2 passing through, NH_3 (3356, 3260, 3165 cm^{-1}) decreased rapidly and completely disappeared at 30 min in simultaneous pre-sorption condition (Fig. 9**c**). But the toluene (*i.e.* methyl group at 2962 and 2886 cm^{-1}) still remained. It was postulated that the reduction and oxidation reactions occurred in sequence, where the NO reduction precedes the toluene oxidation.

To study the interaction between NH_3 and Cu/Ce sites, the adsorption of NH_3 on CuTi, CeTi and CuCeTi at 250 °C (Fig. 9**d**) was analyzed. The bands at 1584–1607, 1306, and 1241 cm^{-1} were attributed to the adsorption of NH_3 on the Lewis acid site, and the bands at 1675 and 1442 cm^{-1} were assigned to the adsorption of NH_3 on the Brønsted acid site. The peaks of Lewis acid and Brønsted acid between 1400 and 1800 cm^{-1} overlapped with the peaks of toluene oxidation intermediates under synergistic conditions, which was difficult to distinguish the change of NH_3. By comparing the peaks below 1400 cm^{-1}, however, the peaks at 1306 and 1241 cm^{-1} on CuCeTi can be attributed to CeTi and CuTi, respectively. To further study the role of Cu and Ce sites to SCR under synergistic conditions, an experiment was designed to observe the changes of NH_3 peaks on Cu and Ce sites through switching on and off the NO stream during *in situ* DRIFTS testing (Fig. 9**e**). When 500 ppm NO was on, the peak area of NH_3 (1306 and 1241 cm^{-1}) decreased because the adsorbed NH_3 was consumed by SCR reaction. When NO was off, the NH_3 peak began to increase as the SCR reaction stopped and NH_3 began to accumulate. Compared with the NH_3 on the Cu site (1241 cm^{-1}), the NH_3 on Ce site (1306 cm^{-1}) was more sensitive to the vibration of NO, which means NH_3 on the Ce site had better interaction with gaseous NO during SCR reaction. Therefore, the Ce site is more likely to participate in SCR in the synergistic reaction.

3.3.3. *Synergistic abatement of toluene and NO_x*

Hydrocarbons can participate in the SCR reaction as reducing agents, also known as HC-SCR. Under synergistic reaction conditions, toluene present in the atmosphere can be consumed by HC-SCR reaction. The intermediate of the HC-SCR reaction is the species with -CN group. In addition, the C-NO group on the benzene ring can undergo faster ring opening through a more electrophilic reaction, thereby enhancing the degradation of toluene [21,51]. However, there were no characteristic peaks of -CN and -NCO in the spectrum of CuCeTi between 2500 and 2000 cm^{-1} (Fig. S28). Furthermore, by replacing NH_3 with C_7H_8 as reducing agent in the SCR reaction, the NO_x conversion was less than 35% even at 400 °C (Fig. S29). Therefore, the HC-SCR reaction rarely occurred on CuCeTi during the synergistic reaction, which means the boosting effect of toluene oxidation is mainly induced by the interaction between the Cu/Ce sites.

Combined with the above research results, the mechanism of toluene and NO synergistic removal was proposed in Scheme 1. Toluene and NH_3 came to the catalyst surface first, toluene exhibited a preference for adsorption on the Cu site. The SCR reaction was priority initiated on Ce site, where the gaseous NH_3 was absorbed on the Lewis acid sites (Ce-NH_3) and Brønsted acid sites (Ce-NH_4^+). After oxidative dehydrogenation, the NH_2 species reacted with gaseous NO to form NH_2NO, and next to give N_2 and H_2O as final product. After SCR reaction, Ce^{3+} was generated and through active site interaction (Cu^+–O–Ce^{4+} ↔ Cu^{2+}–□–Ce^{3+}) oxidation vacancy and Cu^{2+} was also generated [21]. More Cu^{2+} site was beneficial for toluene oxidation as Cu was the main adsorption site for toluene. And oxidation vacancy induced the formation of lattice oxygen through oxygen migration of O_2(gas) → O_2(ads) → O_2^{2-}(ads) → O^{2-}(lattice), where lattice oxygen contributed to ring-opening reaction [52]. Therefore, toluene oxidation was boosted through the pathways of benzyl alcohol, benzaldehyde, benzoic acid, maleic anhydride, small molecule acids, and finally CO_2 and H_2O. In the synergistic reaction with stoichiometric amounts of NH_3 and NO, NH_3 tended to move and to be adsorbed at the Ce site as the SCR reaction occurring at the Ce site will continue to consume NH_3. But the excess amount of NH_3 would inhibit the toluene oxidation. Other possible reaction, such as HC-SCR was not predominated in the reaction process.

4. Conclusions

In summary, a dual-functional CuCeTi catalyst was successfully synthesized by a facile coprecipitation method. CuCeTi exhibited a synergistic NO_x and toluene removal windows over a temperature range of 250–370 °C, and outperformed significantly the corresponding single-component CuTi and CeTi catalysts. The catalyst could sustain the NO_x and VOCs removal efficiencies above 90% even in the presence of 5 vol % H_2O and 500 ppm SO_2 at 300 °C. While NH_3 was found as the main inhibitor for the toluene oxidation, toluene had minimal effect on the

SCR activity of CuCeTi. More strikingly, a promotion of toluene oxidation was observed in the presence of stoichiometric amounts of NH_3 and NO. According to mechanistic studies by *in situ* DRIFTS, the Cu site mainly interacted with toluene and underwent oxidation reaction. While the Ce site played a major role in adsorption of NH_3, and took placed in the SCR reaction. Due to this unique Cu-Ce catalytic site, the interference between pollutants (NO and toluene) can be minimized. Furthermore, the redox cycling between Ce^{4+}/Ce^{3+} and Cu^{2+}/Cu^{+} pairs could facilitate the generation of lattice oxygen and Cu^{2+} and boosting the toluene oxidation. This study may provide new considerations for the rational design of high-performance vanadium-free catalysts toward synergistic NO_x and VOCs abatement.

CRediT authorship contribution statement

Ziyang Guo: Data curation, Investigation, Writing – original draft, Writing – review & editing. **Beilong Lin:** Data curation, Validation. **Yu Huang:** Visualization, Writing – review & editing. **Jiali Tang:** Visualization, Writing – review & editing. **Peirong Chen:** Conceptualization, Formal analysis, Writing – review & editing. **Daiqi Ye:** Formal analysis, Conceptualization. **Yun Hu:** Writing – original draft, Writing – review & editing, Formal analysis, Supervision, Conceptualization.

Declaration of Competing Interest

The authors declare that they have no known competing financial interests or personal relationships that could have appeared to influence the work reported in this paper.

Data availability

No data was used for the research described in the article.

Acknowledgments

This work was supported by the National Key Research and Development Program of China (2022YFB4101500) and the Yancheng City "Yellow Sea Pearl Talent Project" Leading Talent Program.

Appendix A. Supplementary material

The information provided includes catalyst preparation, material characterization, catalytic activity measurements, experimental results with synthesized catalysts under different reaction conditions and *in situ* DRIFTS data.

Appendix A. Supporting information

Supplementary data associated with this article can be found in the online version at doi:10.1016/j.apcatb.2023.123430.

References

[1] S.M. Charan, Y.L. Huang, J.H. Seinfeld, Computational simulation of secondary organic aerosol formation in laboratory chambers, Chem. Rev. 119 (2019) 11912–11944, https://doi.org/10.1021/acs.chemrev.9b00358.
[2] S.L. Nordahl, J.P. Devkota, J. Amirebrahimi, S.J. Smith, H.M. Breunig, C.V. Preble, A.J. Satchwell, L. Jin, N.J. Brown, T.W. Kirchstetter, C.D. Scown, Life-cycle greenhouse gas emissions and human health trade-offs of organic waste management strategies, Environ. Sci. Technol. 54 (2020) 9200–9209, https://doi.org/10.1021/acs.est.0c00364.
[3] C. He, J. Cheng, X. Zhang, M. Douthwaite, S. Pattisson, Z.P. Hao, Recent advances in the catalytic oxidation of volatile organic compounds: a review based on pollutant sorts and sources, Chem. Rev. 119 (2019) 4471–4568, https://doi.org/10.1021/acs.chemrev.8b00408.
[4] R.P. Wang, X.Q. Wang, S.Y. Cheng, K. Wang, L. Cheng, J.X. Zhu, H.S. Zheng, W. J. Duan, Emission characteristics and reactivity of volatile organic compounds from typical high-energy-consuming industries in north China, Sci. Total. Environ. 809 (2022), https://doi.org/10.1016/j.scitotenv.2021.151134.
[5] J.W. Shi, H. Deng, Z.P. Bai, S.F. Kong, X.Y. Wang, J.M. Hao, X.Y. Han, P. Ning, Emission and profile characteristic of volatile organic compounds emitted from coke production, iron smelt, heating station and power plant in liaoning province, China, Sci. Total. Environ. 515 (2015) 101–108, https://doi.org/10.1016/j.scitotenv.2015.02.034.
[6] L.P. Han, S.X. Cai, M. Gao, J. Hasegawa, P.L. Wang, J.P. Zhang, L.Y. Shi, D. S. Zhang, Selective catalytic reduction of NO_x with NH_3 by using novel catalysts: state of the art and future prospects, Chem. Rev. 119 (2019) 10916–10976, https://doi.org/10.1021/acs.chemrev.9b00202.
[7] W.Y. Jiang, Y.L. Yu, F. Bi, P.F. Sun, X.L. Weng, Z.B. Wu, Synergistic elimination of NO_x and chloroaromatics on a commercial V_2O_5-WO_3/TiO_2 catalyst: byproduct analyses and the SO_2 effect, Environ. Sci. Technol. 53 (2019) 12657–12667, https://doi.org/10.1021/acs.est.9b04155.
[8] X. Huang, D. Wang, Q.L. Yang, Y. Peng, J.H. Li, Multi-pollutant control (MPC) of NO and chlorobenzene from industrial furnaces using a vanadia-based SCR catalyst, Appl. Catal. B 285 (2021), https://doi.org/10.1016/j.apcatb.2020.119835.
[9] S.Y. Zhai, Y.T. Su, X.L. Weng, R.N. Li, H.Q. Wang, Z.B. Wu, Synergistic elimination of NO_x and chlorinated organics over VO_x/TiO_2 catalysts: a combined experimental and DFT study for exploring vanadate domain effect, Environ. Sci. Technol. 55 (2021) 12862–12870, https://doi.org/10.1021/acs.est.1c02997.
[10] D. Wang, Q.Z. Chen, X. Zhang, C. Gao, B. Wang, X. Huang, Y. Peng, J.H. Li, C. M. Lu, J. Crittenden, Multipollutant control (MPC) of flue gas from stationary sources using SCR technology: a critical review, Environ. Sci. Technol. 55 (2021) 2743–2766, https://doi.org/10.1021/acs.est.0c07326.
[11] S. Pitkaaho, S. Ojala, T. Maunula, A. Savimaki, T. Kinnunen, R.L. Keiski, Oxidation of dichloromethane and perchloroethylene as single compounds and in mixtures, Appl. Catal. B 102 (2011) 395–403, https://doi.org/10.1016/j.apcatb.2010.12.011.
[12] Y.P. Long, Y.T. Su, Y.H. Xue, Z.B.A. Wu, X.L. Weng, V_2O_5-WO_3/TiO_2 catalyst for efficient synergistic control of NO_x and chlorinated organics: insights into the arsenic effect, Environ. Sci. Technol. 55 (2021) 9317–9325, https://doi.org/10.1021/acs.est.1c02636.
[13] G.F. Xiao, Z.Y. Guo, J.H. Li, Y.Y. Du, Y.L. Zhang, T. Xiong, B.L. Lin, M.L. Fu, D. Q. Ye, Y. Hu, Insights into the effect of flue gas on synergistic elimination of toluene and NO_x over V_2O_5-$MoO_3(WO_3)$/TiO_2 catalysts, Chem. Eng. J. 435 (2022), https://doi.org/10.1016/j.cej.2022.134914.
[14] G.F. Xiao, Z.Y. Guo, B.L. Lin, M.L. Fu, D.Q. Ye, Y. Hu, Cu-VWT catalysts for synergistic elimination of NO_x and volatile organic compounds from coal-fired flue gas, Environ. Sci. Technol. 56 (2022) 10095–10104, https://doi.org/10.1021/acs.est.2c02083.
[15] G.B. Li, L. Wang, P. Wu, S.L. Zhang, K. Shen, Y.P. Zhang, Insight into the combined catalytic removal properties of Pd modification V/TiO_2 catalysts for the nitrogen oxides and benzene by: an experiment and dft study, Appl. Surf. Sci. 527 (2020), https://doi.org/10.1016/j.apsusc.2020.146787.
[16] L. Chen, J.R. Liu, W.F. Hu, J. Gao, J.Y. Yang, Vanadium in soil-plant system: source, fate, toxicity, and bioremediation, J. Hazard. Mater. 405 (2021), https://doi.org/10.1016/j.jhazmat.2020.124200.
[17] I. Song, H. Lee, S.W. Jeon, D.H. Kim, Understanding the dynamic behavior of acid sites on TiO_2-supported vanadia catalysts via operando drifts under SCR-relevant conditions, J. Catal. 382 (2020) 269–279, https://doi.org/10.1016/j.jcat.2019.12.041.
[18] L.M. Ye, P. Lu, X.B. Chen, P. Fang, Y. Peng, J.H. Li, H.B. Huang, The deactivation mechanism of toluene on MnO_x-CeO_2 SCR catalyst, Appl. Catal. B 277 (2020), https://doi.org/10.1016/j.apcatb.2020.119257.
[19] J.J. Liu, X.Y. Shi, Y.B. Yu, M.Y. Zhang, D.R. Liu, H. He, Excellent hydrocarbon tolerance of CeO_2-WO_3-SnO_2 oxide catalyst for the NH_3-SCR of NOx, Appl. Catal. B 324 (2023), https://doi.org/10.1016/j.apcatb.2022.122283.
[20] H.C. Erythropel, J.B. Zimmerman, T.M. de Winter, L. Petitjean, F. Melnikov, C. H. Lam, A.W. Lounsbury, K.E. Mellor, N.Z. Jankovic, Q.S. Tu, L.N. Pincus, M. M. Falinski, W.B. Shi, P. Coish, D.L. Plata, P.T. Anastas, The green chemistree: 20 years after taking root with the 12 principles, Green. Chem. 20 (2018) 1929–1961, https://doi.org/10.1039/c8gc00482j.
[21] H. Liu, J.J. Chen, Y. Wang, R.Q. Yin, W.H. Yang, G.M. Wang, W.Z. Si, Y. Peng, J. H. Li, Interaction mechanism for simultaneous elimination of nitrogen oxides and toluene over the bifunctional CeO_2-TiO_2 mixed oxide catalyst, Environ. Sci. Technol. 56 (2022) 4467–4476, https://doi.org/10.1021/acs.est.1c08424.
[22] C. Zhang, J.P. Zhang, Y.J. Shen, J.B. He, W.Q. Qu, J. Deng, L.P. Han, A.L. Chen, D. S. Zhang, Synergistic catalytic elimination of NO_x and chlorinated organics: Cooperation of acid sites, Environ. Sci. Technol. 56 (2022) 3719–3728, https://doi.org/10.1021/acs.est.1c08009.
[23] M. Gallastegi-Villa, A. Aranzabal, J.A. Gonzalez-Marcos, J.R. Gonzalez-Velasco, G. C.T. Environm, Metal-loaded ZSM-5 zeolites for catalytic purification of dioxin/furans and NO_x containing exhaust gases from mwi plants: effect of different metal cations, Appl. Catal. B 184 (2016) 238–245, https://doi.org/10.1016/j.apcatb.2015.11.006.
[24] P. Djinovic, A. Ristic, T. Zumbar, V.D.B.C. Dasireddy, M. Rangus, G. Drazic, M. Popova, B. Likozar, N.Z. Logar, N.N. Tusar, Synergistic effect of CuO nanocrystals and Cu-oxo-Fe clusters on silica support in promotion of total catalytic oxidation of toluene as a model volatile organic air pollutant, Appl. Catal. B 268 (2020), https://doi.org/10.1016/j.apcatb.2020.118749.
[25] Y.J. Shi, Z.M. Li, J.L. Wang, R.X. Zhou, Synergistic effect of Pt/Ce and USY zeolite in Pt-based catalysts with high activity for vocs degradation, Appl. Catal. B 286 (2021), https://doi.org/10.1016/j.apcatb.2021.119936.

[26] F. Gao, D.H. Mei, Y.L. Wang, J. Szanyi, C.H.F. Peden, Selective catalytic reduction over Cu/SSZ-13: Linking homo- and heterogeneous catalysis, J. Am. Chem. Soc. 139 (2017) 4935–4942, https://doi.org/10.1021/jacs.7b01128.
[27] L.E. Gevers, L.R. Enakonda, A. Shahid, S. Ould-Chikh, C.I.Q. Silva, P.P. Paalanen, A. Aguilar-Tapia, J.L. Hazemann, M.N. Hedhili, F. Wen, J. Ruiz-Martinez, Unraveling the structure and role of Mn and Ce for NO_x reduction in application-relevant catalysts, Nat. Commun. 13 (2022), https://doi.org/10.1038/s41467-022-30679-9.
[28] J. Liu, J.W. Wang, J. Cheng, Y.S. Zhang, T. Wang, W.P. Pan, Distribution and emission of speciated volatile organic compounds from a coal-fired power plant with ultra-low emission technologies, J. Clean. Prod. 264 (2020), https://doi.org/10.1016/j.jclepro.2020.121686.
[29] A. Garg, N.C. Gupta, A comprehensive study on spatio-temporal distribution, health risk assessment and ozone formation potential of BETX emissions in ambient air of Delhi, India, Sci. Total Environ. 659 (2019) 1090–1099, https://doi.org/10.1016/j.scitotenv.2018.12.426.
[30] H. Hao, B.F. Jin, W. Liu, X.D. Wu, F.F. Yin, S. Liu, Robust Pt@ TiO_x/TiO_2 catalysts for hydrocarbon combustion: effects of Pt-TiO_x interaction and sulfates, Acs Catal. 10 (2020) 13543–13548, https://doi.org/10.1021/acscatal.0c03984.
[31] L. Zhang, L. Li, Y. Cao, X. Yao, C. Ge, F. Gao, Y. Deng, C. Tang, L. Dong, Getting insight into the influence of SO_2 on TiO_2/CeO_2 for the selective catalytic reduction of NO by NH_3, Appl. Catal. B 165 (2015) 589–598, https://doi.org/10.1016/j.apcatb.2014.10.029.
[32] H. Liu, Z. Fan, C. Sun, S. Yu, S. Feng, W. Chen, D. Chen, C. Tang, F. Gao, L. Dong, Improved activity and significant SO_2 tolerance of samarium modified CeO2-TiO2 catalyst for NO selective catalytic reduction with NH3, Appl. Catal., B 244 (2019) 671–683, https://doi.org/10.1016/j.apcatb.2018.12.001.
[33] J. Liu, G.Q. Li, Y.F. Zhang, X.Q. Liu, Y. Wang, Y. Li, Novel Ce-W-Sb mixed oxide catalyst for selective catalytic reduction of NO with NH_3, Appl. Surf. Sci. 401 (2017) 7–16, https://doi.org/10.1016/j.apsusc.2016.12.244.
[34] L.G. Li, Q. Shao, X.Q. Huang, Amorphous oxide nanostructures for advanced electrocatalysis, Chem. -Eur. J. 26 (2020) 3943–3960, https://doi.org/10.1002/chem.201903206.
[35] X.S. Huang, G.D. Zhang, F. Dong, Z.C. Tang, An environmentally friendly wide temperature cewtiox catalyst with superior performance for the selective catalytic reduction NO_x with NH_3, J. Ind. Eng. Chem. 69 (2019) 66–76, https://doi.org/10.1016/j.jiec.2018.09.006.
[36] Y.F. Li, T.Y. Chen, S.Q. Zhao, P. Wu, Y.A. Chong, A.Q. Li, Y. Zhao, G.X. Chen, X. J. Jin, Y.C. Qiu, D.Q. Ye, Engineering cobalt oxide with coexisting cobalt defects and oxygen vacancies for enhanced catalytic oxidation of toluene, Acs Catal. 12 (2022) 4906–4917, https://doi.org/10.1021/acscatal.2c00296.
[37] Y.Q. Zeng, T.X. Wang, S.L. Zhang, Y.N. Wang, Q. Zhong, Sol-gel synthesis of CuO-TiO_2 catalyst with high dispersion CuO species for selective catalytic oxidation of NO, Appl. Surf. Sci. 411 (2017) 227–234, https://doi.org/10.1016/j.apsusc.2017.03.107.
[38] A.L. Lu, H.L. Sun, N.W. Zhang, L.M. Che, S.Y. Shan, J. Luo, J.B. Zheng, L.F. Yang, D. L. Peng, C.J. Zhong, B.H. Chen, Surface partial-charge-tuned enhancement of catalytic activity of platinum nanocatalysts for toluene oxidation, Acs. Catal. 9 (2019) 7431–7442, https://doi.org/10.1021/acscatal.9b01776.
[39] M.M. Luo, Y. Cheng, X.Z. Peng, W. Pan, Copper modified manganese oxide with tunnel structure as efficient catalyst for low-temperature catalytic combustion of toluene, Chem. Eng. J. 369 (2019) 758–765, https://doi.org/10.1016/j.cej.2019.03.056.
[40] Y.T. Bai, X. Bian, W.Y. Wu, Catalytic properties of CuO/CeO_2-Al_2O_3 catalysts for low concentration NO reduction with CO, Appl. Surf. Sci. 463 (2019) 435–444, https://doi.org/10.1016/j.apsusc.2018.08.229.
[41] L. Meng, H. Zhao, Low-temperature complete removal of toluene over highly active nanoparticles CuO-TiO_2 synthesized via flame spray pyrolysis, Appl. Catal. B: Environ. 264 (2020), 118427, https://doi.org/10.1016/j.apcatb.2019.118427.
[42] W. Shan, F. Liu, H. He, X. Shi, C. Zhang, Novel cerium–tungsten mixed oxide catalyst for the selective catalytic reduction of NO_x with NH_3, Chem. Commun. 47 (2011) 8046–8048, https://doi.org/10.1039/C1CC12168E.
[43] J. Li, Y.X. Han, Y.H. Zhu, R.X. Zhou, Purification of hydrogen from carbon monoxide for fuel cell application over modified mesoporous CuO-CeO_2 catalysts, Appl. Catal. B 108 (2011) 72–80, https://doi.org/10.1016/j.apcatb.2011.08.010.
[44] C. He, Y.K. Yu, L. Yue, N.L. Qiao, J.J. Li, Q. Shen, W.J. Yu, J.S. Chen, Z.P. Hao, Low-temperature removal of toluene and propanal over highly active mesoporous $CuCeO_x$ catalysts synthesized via a simple self-precipitation protocol, Appl. Catal. B 147 (2014) 156–166, https://doi.org/10.1016/j.apcatb.2013.08.039.
[45] J.H. Lu, J.P. Zhong, Q.M. Ren, J.Q. Li, L.H. Song, S.P. Mo, M.Y. Zhang, P.R. Chen, M.L. Fu, D.Q. Ye, Construction of Cu-Ce interface for boosting toluene oxidation: study of Cu-Ce interaction and intermediates identified by in situ drifts, Chin. Chem. Lett. 32 (2021) 3435–3439, https://doi.org/10.1016/j.cclet.2021.05.029.
[46] C.Z. Wang, F.Y. Gao, S.J. Ko, H.H. Liu, H.H. Yi, X.L. Tang, Structural control for inhibiting SO_2 adsorption in porous MnCe nanowire aerogel catalysts for low-temperature NH_3-SCR, Chem. Eng. J. 434 (2022), https://doi.org/10.1016/j.cej.2022.134729.
[47] L. Zhao, Y. Huang, J. Zhang, L. Jiang, Y. Wang, Al_2O_3-modified CuO-CeO_2 catalyst for simultaneous removal of NO and toluene at wide temperature range, Chem. Eng. J. 397 (2020), 125419, https://doi.org/10.1016/j.cej.2020.125419.
[48] X.X. Wang, Y. Shi, S.J. Li, W. Li, Promotional synergistic effect of Cu and Nb doping on a novel Cu/Ti-Nb ternary oxide catalyst for the selective catalytic reduction of NO_x with NH_3, Appl. Catal. B 220 (2018) 234–250, https://doi.org/10.1016/j.apcatb.2017.08.021.
[49] G.B. Li, K. Shen, L. Wang, Y.P. Zhang, H.Q. Yang, P. Wu, B. Wang, S.L. Zhang, Synergistic degradation mechanism of chlorobenzene and NO_x over the multi-active center catalyst: the role of NO_2, Bronsted acidic site, oxygen vacancy, Appl. Catal. B 286 (2021), https://doi.org/10.1016/j.apcatb.2020.119865.
[50] W.J. Zhang, Y. Zhong, Q. Wang, D.K. Shen, G.F. Liu, Comparison study of the SCR performance over Mn-TiO_2 and Ce-TiO_2 catalysts: an experimental and DFT study, Energy Fuel 35 (2021) 14681–14691, https://doi.org/10.1021/acs.energyfuels.1c02170.
[51] P. Lu, Y.M. Ye, X.H. Yan, X.B. Chen, P. Fang, D.Y. Chen, D.S. Chen, C.P. Cen, N_2O inhibition by toluene over Mn-Fe spinel SCR catalyst, J. Hazard. Mater. 414 (2021), https://doi.org/10.1016/j.jhazmat.2021.125468.
[52] L. Ye, P. Lu, Y. Xianhui, H. Huang, Boosting simultaneous catalytic removal of NO_x and toluene via cooperation of Lewis acid and oxygen vacancies, Appl. Catal. B 331 (2023), 122696, https://doi.org/10.1016/j.apcatb.2023.122696.